American Mineralogist, Volume 104, pages 580–587, 2019

High-pressure behavior of liebenbergite: The most incompressible olivine-structured silicate

Dongzhou Zhang[1,2,*], Yi Hu[3], Jingui Xu[4], Robert T. Downs[5], Julia E. Hammer[6], and Przemyslaw K. Dera[1,3]

[1]Hawaii Institute of Geophysics and Planetology, University of Hawaii at Manoa, Honolulu, Hawaii 96822, U.S.A.
[2]GeoSoilEnviroCARS, University of Chicago, Lemont, Illinois 60439, U.S.A. Orcid 0000-0002-6679-892X
[3]Department of Geology and Geophysics, University of Hawaii at Manoa Honolulu, Hawaii 96822, U.S.A.
[4]Key Laboratory of High-Temperature and High-Pressure Study of the Earth's Interior, Institute of Geochemistry, Chinese Academy of Sciences, Guiyang, Guizhou 550081, China
[5]Department of Geosciences, University of Arizona, Tucson, Arizona 85721, U.S.A
[6]Department of Geology and Geophysics, University of Hawaii at Manoa Honolulu, Hawaii 96822, U.S.A. Orcid 0000-0002-5977-2932

Abstract

Nickel is an abundant element in the bulk earth, and nickel-dominant olivine, liebenbergite, is the only igneous nickel-rich silicate found in nature. In this study, we used high-pressure single-crystal diffraction to explore the compressional behavior of a synthetic liebenbergite sample up to 42.6 GPa at ambient temperature. Over the studied pressure range, the liebenbergite sample retains the orthorhombic *Pbnm* structure, and no phase transition is observed. A third-order Birch-Murnaghan equation of state was used to fit the pressure behavior of the unit-cell volume, lattice parameters, the polyhedral volume, and the average bond length within each polyhedron. The best-fit bulk modulus K_{T0} = 163(3) GPa and its pressure derivative K'_{T0} = 4.5(3). We find that liebenbergite is the most incompressible olivine-group silicate reported thus far, and Ni^{2+} tends to increase the isothermal bulk modulus of both olivine- and spinel-structured silicates. Consequently, Ni-rich olivine has a higher density compared to Ni-poor olivine at the upper mantle *P-T* conditions; however enrichment of Ni in mantle olivine is generally too low to make this density difference relevant for fractionation or buoyancy.

Keywords: Olivine, Ni, high pressure, equation of states, single-crystal diffraction

Introduction

Nickel is the most abundant of the minor elements in the bulk earth. It is less common than iron, oxygen, silicon, and magnesium, which make up 94% of the atoms in the Earth, yet slightly more common than calcium and aluminum (McDonough and Sun 1995; Allegre et al. 2001). A geochemical study of the distribution of nickel in the Earth can constrain our understanding of the Earth's evolution, for example, core segregation (Ringwood 1959; Siebert et al. 2012; Fischer et al. 2015). Though one cannot directly measure the composition of the Earth's core, it is estimated that the core contains ~5 wt% nickel, and the core is the largest reservoir of this element (McDonough 2014). This estimate is based on two premises: (1) the assumption that the abundance of nickel in the bulk earth is chondritic, and (2) the calibrated relationship between nickel concentration in mantle rocks and their MgO content (McDonough and Sun 1995; McDonough 2014; Palme and O'Neill 2014). However, most of the research on the nickel concentration in mantle rocks has thus far focused on the shallow materials (McDonough and Sun 1995; Korenaga and Kelemen 2000; Matzen et al. 2013; Palme and O'Neill 2014), and the partitioning coefficients of nickel between minerals and melts are strongly influenced by pressure (Li and Agee 1996; Siebert et al. 2012; Matzen et al. 2013, 2017; Fischer et al. 2015; Pu et al. 2017). Under certain geological settings, nickel could be enriched in mantle minerals without directly interacting with the Earth's core (Ishimaru and Arai 2008; Straub et al. 2008; Matzen et al. 2013), so it is possible to have some nickel-rich reservoir in the deep part of the silicate mantle.

To quantify the possibility of deep reservoirs of Ni-rich silicates, one needs to understand the high-pressure behavior of nickel-rich silicates. Systematic research on Ni-rich silicates is still lacking. From a mineralogical perspective, one cannot assume that nickel behaves the same as iron in silicates. For example, there are no nickel end-members of garnet and pyroxene (Back et al. 2017; Burns 1973; Campbell and Roeder 1968; Gentile and Roy 1960), while iron end-members of garnet (almandine) and pyroxene (ferrosilite) both exist. Nickel is highly compatible with mantle peridotites (Griffin et al. 1989; Hart and Davis 1978; Mysen 1979; Palme and O'Neill 2014). Geological surveys show that nickel tends to be enriched in olivine under natural conditions (Ishimaru and Arai 2008; Straub et al. 2008), and liebenbergite, the nickel end-member of olivine (De Waal and Calk 1973), is the only igneous nickel-rich silicate found in nature (Supplemental[1] Table S1, Back et al. 2017). Considering the abundance of olivine in the mantle, studying the high-pressure behavior of liebenbergite will provide insights into nickel-bearing silicates at deep earth conditions.

Studies, described below, were previously carried out to constrain the phase diagram and stability field of liebenbergite.

* E-mail: dzhang@hawaii.edu

At high pressures and temperatures (P > ~4 GPa, T > 700 °C), the olivine-structured liebenbergite transforms into a cubic spinel (Ringwood 1962; Akimoto et al. 1965; Akaogi et al. 1982). At even higher pressures (P > 14 GPa, T > 1400 °C), the Ni_2SiO_4 spinel decomposes into bunsenite (NiO) and stishovite (SiO_2) (Liu 1975). The pressure-volume equation of state and elasticity of Ni_2SiO_4 spinel have previously been reported (Mao et al. 1969; Sato 1977b; Finger et al. 1979; Bass et al. 1984; Hazen 1993). The elasticity of liebenbergite measured at ambient conditions by Brillouin spectroscopy has also been reported (Bass et al. 1984). One high-pressure Raman study has been carried out on liebenbergite to 35 GPa, and a phase transition was observed around 30 GPa in non-hydrostatic pressure environment (no pressure medium), yet the transition was not observed when water was used as the pressure medium (Lin 2001). Surprisingly, no compressional equation of state study has been carried out on liebenbergite. In this report, we present our experimental results on the compressional equation of state measurement of liebenbergite up to 42.6 GPa at room temperature.

Experiments

The liebenbergite sample measured in this study was synthesized using the flux method (Ozima 1976). Electron microprobe analysis conducted on a Cameca SX100 instrument at the University of Arizona determined the chemical composition of the sample as $Ni_{2.009}Si_{0.995}O_4$. Raman spectrum in the range of 200–5500 cm^{-1} suggests that the sample is anhydrous. A 15 × 15 × 5 μm fragment of liebenbergite was mounted onto a polymer holder for room-pressure measurement. Then, the same crystal was loaded into a 4-pin DAC with a ~ ±34° opening angle. Helium was used as the pressure medium (Rivers et al. 2008), and gold was used to calibrate the pressure of the sample (Fei et al. 2007). The diffraction data were collected at the experimental station 13-BM-C of the Advanced Photon Source, Argonne National Laboratory, and the experimental details were described previously (Zhang et al. 2016a, 2017). The crystal structure refinements were carried out with the ATREX/RSV, SHELXL, Olex2, and VESTA software packages (Sheldrick 2008; Momma and Izumi 2008; Dolomanov et al. 2009; Dera et al. 2013). We used isotropic atomic displacement parameters (U_{iso}) for all atoms. The crystal structure model of Lager and Meagher (1978) was used to initialize the refinement. The crystal structure of liebenbergite is illustrated in S1. Figures of merits of the refinements, unit-cell parameters, atomic coordinates Supplemental[1] Figure and displacement parameters, bond lengths, polyhedral volumes, and distortions at different pressures are given in Table 1, Supplemental[1] Tables S2 and S3, and the CIF[1].

Data analysis

Liebenbergite, the most incompressible olivine-structured silicate

Throughout the investigated pressure range (1 bar to 42.6 GPa), the liebenbergite sample retains the *Pbnm* olivine structure. The compression curve of the liebenbergite sample does not show any abrupt changes, consistent with the absence of structural transitions during compression. We fit the P-V compression curve of our sample with a third-order Birch-Murnaghan (BM3) equation of state (Fig. 1) using the EoSFit7c software package (Angel et al. 2014). The best-fit parameters are: V_0 = 283.38(7) $Å^3$, K_{T0} = 163(3) GPa, and K'_{T0} = 4.5(3). The K_{T0} of liebenbergite is significantly higher than K_{T0} of forsterite (Mg_2SiO_4, 123–136 GPa, Supplemental Table S4) and fayalite (Fe_2SiO_4, 125–136 GPa, Supplemental Table S4). The K_{T0} of liebenbergite is consistent with the adiabatic bulk modulus (K_{S0}) measured from Brillouin spectroscopy [165(2) GPa, Bass et al. 1984].

We also used the pressure-axial length BM3 equations of state to fit the lattice parameters a, b, and c (Fig. 2). The axial compressibilities were calculated from the best-fit linear moduli. The BM3 fitting was carried out with EoSFit 7c software (Angel et al. 2014). The best-fit BM3 parameters are listed in Table 2. The liebenbergite crystal shows elastic anisotropy on compression. At ambient pressure, the axial compressibilities of the three axes are: β_a = 1.47(2) TPa^{-1}, β_b = 2.63(2) TPa^{-1}, and β_c = 2.14(1) TPa^{-1}. The ratio between the three axes using the BM3 fitting is β_a:β_b:β_c = 1.00:1.79:1.46. The **a**-axis is most incompressible, and the **b**-axis is the most compressible axis. The axial compressibility can also be calculated with the following equation:

$$\beta_i = \sum_j s_{ij} \quad (1)$$

where s_{ij} is the elastic compliance of the mineral (Speziale et al. 2004). Using the adiabatic elastic compliances reported by (Bass et al. 1984), the axial compressibilities are calculated as: β_a = 1.4(1) TPa^{-1}, β_b = 2.5(1) TPa^{-1}, and β_c = 2.2(1) TPa^{-1}. The axial compressibilities measured from our study are consistent

Table 1. Details of each polyhedron of liebenbergite at different pressures

P (GPa)	0.0001	0.4(2)	3.9(3)	11.7(2)	20.0(1)	25.2(3)	31.4(2)	37.3(2)	42.6(5)
Ni1 Average bond length (A)	2.0803	2.0799	2.0637	2.0417	2.0185	2.0052	1.9838	1.9789	1.9655
Polyhedral volume (A^3)	11.58(5)	11.55(13)	11.30(13)	10.98(15)	10.62(12)	10.42(14)	10.10(11)	10.04(15)	9.87(19)
Distortion index	0.00882	0.00742	0.01431	0.00976	0.01221	0.00808	0.01057	0.00955	0.00496
Quadratic elongation	1.0244	1.0255	1.0247	1.0226	1.0219	1.0212	1.0208	1.0191	1.017
Bond angle variance	86.7801	90.8953	86.9672	79.9342	77.2471	75.1582	72.9187	66.9515	59.8429
Effective coordination number	5.9822	5.9874	5.9474	5.9742	5.9652	5.9848	5.9654	5.9726	5.9941
Bond valence	2.0071	2.0088	2.0950	2.1970	2.3125	2.3749	2.4997	2.5098	2.5775
Ni2 Average bond length (A)	2.1007	2.0982	2.0807	2.0498	2.0188	2.0021	1.9919	1.9732	1.9605
Polyhedral volume (A^3)	12.00(6)	11.96(15)	11.67(15)	11.19(18)	10.74(14)	10.48(16)	10.33(13)	10.06(18)	9.89(19)
Distortion index	0.02519	0.02692	0.02488	0.02643	0.02357	0.02488	0.02309	0.02553	0.02313
Quadratic elongation	1.0209	1.0209	1.0198	1.0179	1.0152	1.0147	1.014	1.0128	1.0114
Bond angle variance	72.374	71.9435	69.0663	61.6849	52.236	50.0929	48.1016	43.6025	38.3159
Effective coordination number	5.8269	5.8053	5.8477	5.8188	5.8423	5.842	5.8602	5.8402	5.8558
Bond valence	1.9232	1.9371	2.0135	2.1676	2.3281	2.4187	2.4602	2.5688	2.6397
Si Average bond length (A)	1.6417	1.6400	1.6357	1.6232	1.6152	1.6061	1.6019	1.5959	1.5974
Polyhedral volume (A^3)	2.23(1)	2.23(4)	2.21(4)	2.16(4)	2.12(3)	2.08(4)	2.06(3)	2.04(5)	2.04(6)
Distortion index	0.00632	0.00592	0.00583	0.00703	0.01173	0.007	0.01059	0.01243	0.01425
Quadratic elongation	1.0113	1.0112	1.0115	1.0122	1.0131	1.0136	1.0149	1.0137	1.0157
Bond angle variance	49.972	48.656	49.9954	53.8924	56.9767	60.1616	63.6643	58.4235	69.3632
Effective coordination number	3.989	3.9937	3.9946	3.9895	3.9784	3.9899	3.9838	3.9779	3.9635
Bond valence	3.8156	3.8305	3.8598	3.9518	4.0016	4.0704	4.0900	4.1171	4.0829

Notes: The average bond length and the polyhedral volume are calculated by the Vesta software (Momma and Izumi 2008). The bond valence is defined by Equation 4. The distortion index is defined by Equation 5. The bond angle variance is defined by Equation 6. The quadratic elongation is defined in Robinson et al. (1971) and has the same trend as the bond angle variance.

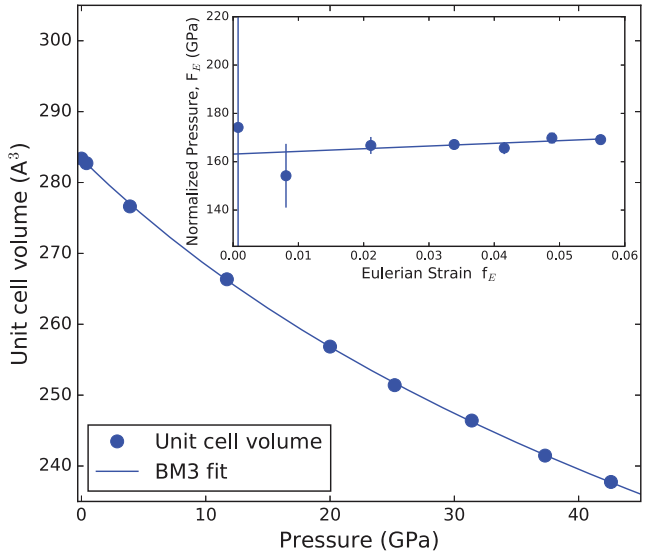

FIGURE 1. Unit-cell volume compression curve of liebenbergite and the best-fit BM3 pressure-volume equation of state. The error bars are smaller than the symbol. BM3 fitting is carried out by the EoSFit7c software package (Angel et al. 2014) Inset: the Eulerian strain-normalized pressure (*f*-*F*) plot. The linear trend of the *f*-*F* plot indicates that the BM3 fitting is suitable (Angel 2000). (Color online.)

with the results determined by Brillouin spectroscopy. The relative axial compressibility of liebenbergite is close to that of forsterite (Mg_2SiO_4, β_a:β_b:β_c = 1.00:1.99:1.55, Downs et al. (1996), β_a:β_b:β_c = 1.0:2.2:1.6, Finkelstein et al. 2014), fayalite (Fe_2SiO_4, β_a:β_b:β_c = 1.00:2.44:1.30, Zhang 1998), tephroite (Mn_2SiO_4, β_a:β_b:β_c = 1.00:2.40:1.36, Zhang 1998) and Co-olivine (β_a:β_b:β_c = 1.00:2.26:1.61, Zhang 1998).

The isothermal bulk modulus of liebenbergite is 163(3) GPa, which is significantly higher than forsterite (Mg_2SiO_4,

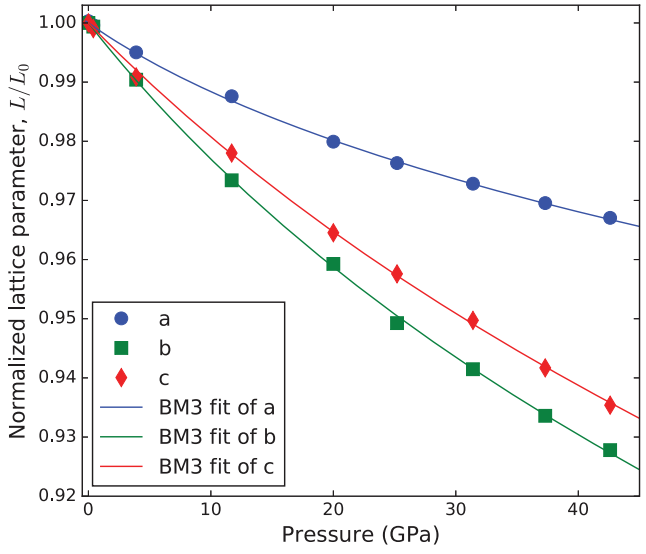

FIGURE 2. Normalized lattice parameters of liebenbergite as functions of pressure, with best-fit BM3 equations of states. BM3 fitting is carried out by the EoSFit7c software package (Angel et al. 2014). (Color online.)

TABLE 2. Best-fit volumetric and linear BM3 parameters of the liebenbergite unit cell, its component polyhedra, lattice parameters, and the average bond lengths of each polyhedron

Volumetric	V_0 (Å^3)	K_{T0} (GPa)	K'_{T0}
Unit-cell volume	283.38(7)	163(3)	4.5(3)
Ni1 octahedron	11.58(5)	191(11)	3.8(8)
Ni2 octahedron	11.99(5)	140(8)	4.8(8)
Si tetrahedron	2.23(1)	300(4)	8(4)
Axial	L_0 (A)	M_{T0} (GPa)	M'_{T0}
Lattice parameter *a*	4.72963(6)	682(7)	41(1)
Lattice parameter *b*	10.1256(8)	380(3)	10.6(2)
Lattice parameter *c*	5.9151(6)	468(2)	9.8(1)
<Ni1-O>	2.080(3)	5.6(3)×10^2	10(2)
<Ni2-O>	2.101(3)	4.0(2)×10^2	13(2)
<Si-O>	1.6419(3)	9(1)×10^2	32(16)

Note: BM3 fitting is carried out by the EoSFit7c software package (Angel et al. 2014).

K_{0T} = 124–136 GPa), tephroite (Mn_2SiO_4, K_{0T} = 125.2 GPa), fayalite (Fe_2SiO_4, K_{0T} = 113–136 GPa), Co-olivine (K_{0T} = 144 GPa), monticellite ($CaMgSiO_4$, K_{0T} = 113 GPa), and LiSc-olivine (K_{0T} = 118 GPa) (Supplemental[1] Table S4 and Fig. 3). The increase in the bulk modulus appears to be related to the compressibility of the **b**-axis, as reviewed above. An increase of Ni^{2+} in the olivine structure increases the isothermal bulk modulus. Similar to olivine, Ni-end-member of spinel also has a higher isothermal bulk modulus than the Mg-, Fe-, and Co-end-members of spinel (Fig. 3). Previous Brillouin study has shown that liebenbergite has larger elastic moduli than other silicate olivines (Bass et al. 1984), which is consistent with our conclusion.

The large isothermal bulk modulus of liebenbergite is probably related to the small ionic radius of Ni^{2+}. Among all divalent cations, Ni^{2+} has the second smallest ionic radius, only larger than Be^{2+} (Shannon 1976). Be^{2+} is too small to stay in the octahedral sites of olivine (Jollands et al. 2016), so Ni^{2+} is the smallest divalent cation that occupies the MO_6 octahedron in olivine. The bulk modulus is found to be related to the specific volume of a mineral. For an ionic crystal with Born power law repulsive potential, it can be proven mathematically that the product of bulk modulus (K) and the specific volume (V_0) of a mineral is a constant (Anderson and Anderson 1970). The Anderson model is deduced from the harmonic approximation, so it is a first-order approximation for the closest-packed arrangement of ions (Anderson and Anderson 1970), and olivine-structured mineral is known to have such closest-packed ionic arrangement (Thompson and Downs 2001). Hazen and Finger (1979) established a similar relationship between polyhedral bulk modulus (K_p) and the polyhedral average bond length (d) in silicates and oxides as follows:

$$K_p d^3/Z_c = 7.5 \pm 0.2 \text{ Mbar}\cdot\text{Å}^3 \quad (2)$$

where Z_c is the cation formal charge. With this reasoning, the NiO_6 octahedron, with the smallest volume and the shortest average bond length, should be the most incompressible octahedron among all divalent cation MO_6 octahedra. It has been suggested that the compressibility of the olivine-structured silicate is dominantly controlled by the compressibility of the MO_6 octahedron (Bass et al. 1984), and therefore liebenbergite tends to be more incompressible than other olivine-structured silicates.

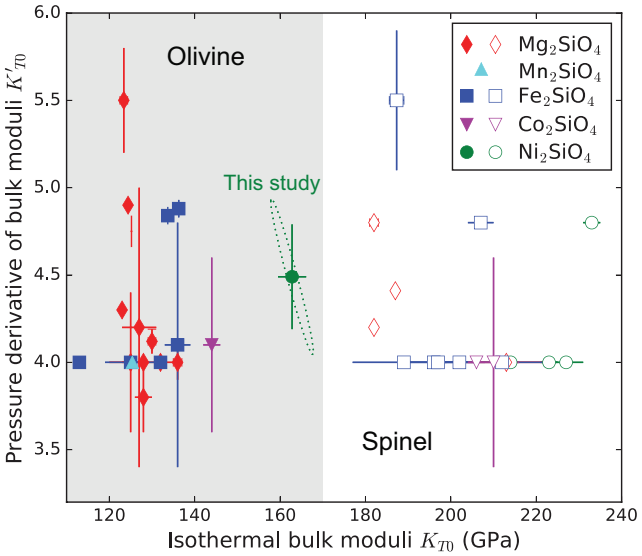

FIGURE 3. Isothermal bulk moduli and their pressure derivatives of different olivine- and spinel-structured silicates. Solid symbols = olivine-structured silicates. Empty symbols = spinel-structured silicates. The 1σ confidence eclipse of K_{T0} and K'_{T0} of this study is shown as the dotted ellipse. Data and references can be found in Supplemental[1] Table S4. (Color online.)

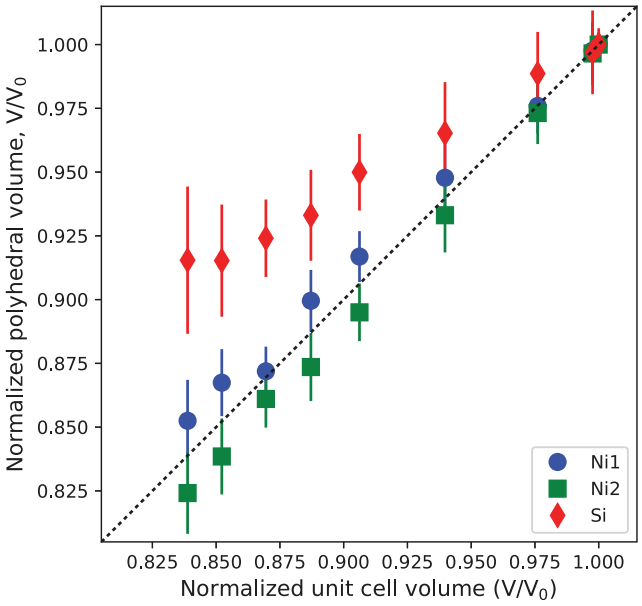

FIGURE 4. Normalized polyhedral volume compared to a normalized unit-cell volume at different pressures. The black dotted line is the Y = X identity line. The Ni1 and Ni2 octahedra shrink simultaneously with the unit cell, yet the Si tetrahedra shrink less than the unit-cell volume at high pressures. (Color online.)

Compressional behavior of each polyhedron in liebenbergite

There are three filled polyhedral sites within the closest-packed array of oxygen atoms in liebenbergite, namely the Ni1 octahedron, the Ni2 octahedron, and the Si tetrahedron. Our crystal structural refinement suggests that the Ni1 and Ni2 octahedra undertake most of the volumetric compression of the crystal, and Ni1 is more incompressible than Ni2 (Fig. 4). The Si tetrahedron has a much smaller polyhedral volume and is significantly more incompressible than both NiO_6 octahedra (Fig. 4). We fit the *P*-*V* compression curves of the three polyhedra with BM3 equation of state (Supplemental[1] Fig. S2). The fits are weighted by the pressure and volumetric errors of the polyhedra, and the volumetric errors of the polyhedra are estimated using the following equation:

$$\delta V_i = 3\frac{\delta a_i}{a_i}V_i \quad (3)$$

where V_i is the volume of each polyhedron, and $<a_i>$ is the average bond length of this polyhedron. The error of the average bond length of each polyhedron is calculated using the Vesta software (Momma and Izumi 2008). The best-fit parameters are listed in Table 2. In many silicates where Si tetrahedra form chains or frameworks, the volume of the Si tetrahedra stays almost constant during the initial compression, because most of the volume compression of the unit cell is accommodated by the rigid body tilting of the Si tetrahedra (e.g., Xu et al. 2017). The Si tetrahedral volume of liebenbergite decreases simultaneously as the compression begins, and we did not observe a stagnant Si tetrahedral volume during the initial compression in liebenbergite. The non-stagnant tetrahedra have been observed in other nesosilicates, such as fayalite (Zhang et al. 2016b) and Ti-clinohumite (Qin et al. 2017), and it comes from the fact that Si tetrahedra are not connected in nesosilicates. The behavior of the normalized average bond length is similar to the polyhedral volume (Supplemental[1] Fig. S3). We fit the pressure vs. average bond length compression curves of the three polyhedra using BM3 equation of state (Table 2). Within the scattering of our data, we did not find any abrupt change in either the polyhedral volume or the average bond length. Bond valence is a physical quantity that estimates the oxidation states of atoms (Brown et al. 2003; Bickmore et al. 2017). Bond valence is defined as:

$$V = \sum \exp\left(\frac{R_0 - R_i}{b}\right) \quad (4)$$

where V is the bond valence, R_0 is a tabulated parameter expressing the ideal bond length between two given atoms (for Ni-O bond, R_0 = 1.675 Å, for Si-O bond, R_0 = 1.624 Å), R_i is the measured bond length, and b = 0.37 Å is an empirical constant (Brown et al. 2003). From the bond length data (Supplemental[1] Table S3), we calculated the bond valence of each cation (Table 1). The bond valences of cations all increase with pressure, indicating that the Ni-O and Si-O bonds are stronger at high pressures.

The distortion of different polyhedra can be described by two parameters, namely the distortion index and the bond angle variance. Distortion index (D) describes the average deviation of the cation-oxygen bond lengths from their mean (Baur 1974; Momma and Izumi 2008) and is defined as:

$$D = \frac{1}{n}\sum_{i=1}^{n}\frac{|l_i - l_{avg}|}{l_{avg}} \quad (5)$$

where l_i is the distance from the central cation to the ith coordinating oxygen, and l_{avg} is the average bond length. Supplemental[1]

Figure S4 shows the evolution of distortion indices of different polyhedra with pressure. Within the scattering of the data, we did not find any systematic change in the distortion indices of the two octahedra, yet the distortion index of the Si-tetrahedron increases with pressure. The distortion index of the Ni1 site is always lower than that of the Ni2 site, which is consistent with previous observations that the M1 site in olivine is less distorted in interatomic distances (Birle et al. 1968).

For polyhedra with a regular shape, i.e., octahedra and tetrahedra, the deviation from the ideal polyhedral shape can be described by the bond angle variance (σ^2) (Momma and Izumi 2008; Robinson et al. 1971). σ^2 is defined as:

$$\sigma^2 = \frac{1}{m-1}\sum_{i=1}^{m}\left(\phi_i - \phi_0\right)^2 \quad (6)$$

where m is the number of O-M-O or O-T-O bond angles (3/2 times of the number of faces in the polyhedron), ϕ_i is the ith bond angle, and ϕ_0 is the ideal bond angle for a perfect regular polyhedron. For perfect regular polyhedra, $\sigma^2 = 0$. We calculate the σ^2 of the octahedra and the tetrahedra at different pressures (Supplemental[1] Fig. S5, Table 1). In the investigated pressure range, the σ^2 of both octahedra systematically decrease, yet the σ^2 of the Si-tetrahedron increases with pressure. The σ^2 of the Ni1 site is always higher than that of the Ni2 site, which is consistent with previous observations that the M1 site in olivine is more distorted in bond angle than the M2 site (Birle et al. 1968). The pressure dependence of σ^2 indicates that the Ni1 and Ni2 octahedra become more regular in bond angle during compression, yet the Si tetrahedron becomes more and more irregular.

After assessing both the distortion index and the bond angle variance, we conclude that both the Ni1 and the Ni2 octahedra exhibit a trend toward an ideal octahedral shape at higher pressure. Similar behavior has been observed in the MgO_6 octahedra of forsterite up to 48 GPa (Finkelstein et al. 2014). Compared to the low transition pressure between olivine- and spinel-structured Ni_2SiO_4 (2–4 GPa, Liu 1975), it is known that Mg^{2+} shifts the olivine transition pressure to ~13 GPa, and Mg-rich olivine is the dominant phase in the Earth's upper mantle (Frost 2008). The solid solution of liebenbergite in Mg-rich olivine is more relevant to the Earth's upper mantle. Ni^{2+} is more compatible with olivine than with melt at the mantle conditions (Matzen et al. 2013, 2017; Pu et al. 2017). Burns (1973) concludes that Ni^{2+} has relatively high crystal field stabilization energy in octahedral coordination, and therefore the octahedral sites in silicate solids are more favorable to accommodate Ni^{2+}, i.e., with a large equilibrium partitioning coefficient over silicate melt.

IMPLICATIONS

Olivine is the most abundant mineral in the Earth's upper mantle. The concentration of Ni in upper mantle olivine is constant at different occurrences (about 0.4 wt% NiO at Fo# (100×Mg/[Mg+Fe]) ≈ 90, Ishimaru and Arai 2008; Sato 1977a). However, under certain geological settings, Ni concentration in olivine can be significantly higher than 0.4 wt%. Ni is found to be enriched in the olivine phenocrysts of the Hawaiian tholeiitic lava (0.25–0.60 wt% NiO, Lynn et al. 2017), and the origin for the Ni enrichment in Hawaiian olivine phenocryst is still under debate. It is possible that pryoxenite melting in the magma source leads to the Ni enrichment in the olivine phenocryst (Herzberg 2006; Herzberg et al. 2016; Sobolev et al. 2007), while other researchers argue that the melting of periodotite at elevated pressure-temperature conditions could also generate olivine with enriched Ni (Matzen et al. 2013; Putirka et al. 2011). Besides the Hawaii hotspot, Ni-rich olivine with NiO content up to 5 wt% has been found in a peridotite xenolith from the Kamchatka volcanic arc in Russia, which is likely due to the diffusion from Ni-rich sulfide melt (Ishimaru and Arai 2008). Natural olivine with the highest Ni concentration ($Ni_{1.52}Mg_{0.33}Co_{0.05}Fe_{0.12}Si_{0.99}O_4$) has been found in the Barberton impact crater in South Africa, and it originates from a Ni-rich meteorite impact event (De Waal and Calk 1973).

Except for the rare meteorite impact events, most Ni-rich olivine is associated with volcanoes. The previous study has suggested that mantle magma accumulation can occur as deep as 100 km (Clague 1987), and melts in the mantle is olivine saturated for its entire journey to the surface (Herzberg 1992). The density of Ni-rich olivine crystals at variable *P-T* conditions helps to estimate the force balance of olivine phenocryst crystallized in magma. We assess the density of olivine crystals with different compositions using the following approach. We use the parameterized isothermal equation of state from Angel et al. (2018) to calculate the density of olivine at different *P-T* conditions.

$$P(V,T) = \frac{3}{2}K_T(T,0)\left[\left(\frac{V_{0T}}{V}\right)^{7/3} - \left(\frac{V_{0T}}{V}\right)^{5/3}\right] \times \left\{1 + \frac{3}{4}\left(K_T'(T,0) - 4\right)\left[\left(\frac{V_{0T}}{V}\right)^{2/3} - 1\right]\right\}$$

$$V(T) = V_0\left[1 - \delta_T + \delta_T\left(1 - \frac{\left(\delta_T{}^2 - 1\right)}{\delta_T}A\right)^B\right]$$

$$A = \alpha_{V,0}\left(\frac{\theta_E}{\xi_0}\right)\left(\frac{1}{\exp\left(\theta_E/T\right)-1} - \frac{1}{\exp\left(\theta_E/T_{ref}\right)-1}\right)$$

$$B = \frac{1}{\delta_T^2 - 1} \quad (7)$$

$$\xi_0 = \frac{(\theta_E/T)^2\exp(\theta_E/T)}{\left(\exp\left(\frac{\theta_E}{T}\right)-1\right)^2}$$

$$K_T(T,0) = K_{T0}\left[\frac{V_0}{V(T)}\right]^{\delta_T}$$

$$K_T'(T,0) = K_{T0}'\left[\frac{V(T)}{V_0}\right]^{\delta'}$$

In the equations above, the parameter θ_E = 484 K is the characteristic Einstein temperature of olivine, δ_T = 5.77 is the

Anderson-Gruneisen parameter, and $\delta' = -3.5$ is a parameterized constant (Angel et al. 2018). In the calculation, we focus on three minerals and their solid solutions: forsterite (Mg_2SiO_4), fayalite (Fe_2SiO_4), and liebenbergite. We calculated the densities of pure forsterite, $(Mg_{0.9}Fe_{0.1})_2SiO_4$, $(Mg_{0.895}Fe_{0.099}Ni_{0.006})_2SiO_4$ (0.6 wt% NiO), and $(Mg_{0.855}Fe_{0.095}Ni_{0.05})_2SiO_4$ (5 wt% NiO) as functions of the depth to 300 km. The pressure-density equation of state parameters for fosterite and fayalite (K_T, K_T', and V_0) are taken from Finkelstein et al. (2014) and Zhang et al. (2016), respectively. The unit-cell volume of solid solution at zero-pressure (V_0) is treated as the Voigt average of the three end-members, as a room-pressure measurement has suggested very little excess volume effect in the olivine solid solution (Bostrom 1987). The bulk modulus of the solid solution (K_{T0}) is treated as the Reuss average of the end-members, which is a good estimate when the crystal is under hydrostatic stress (Angel et al. 2018). We fix the pressure derivative of bulk modulus at 300 K (K_T') as 4.51, which is the best-fit value for the olivine with a mantle composition (Angel et al. 2018) and is close enough to our best-fit K' value of liebenbergite (4.5). We use the upper mantle geotherm profile from Anderson (1982) to correct the thermal effects, and the pressure-depth relationship is adopted from the PREM model (Dziewonski and Anderson 1981). The calculated density of olivine at different depths is illustrated in Figure 5. From our calculations, we conclude that adding Ni to olivine would increase the density of olivine at the upper mantle conditions. Compared to the typical mantle olivine whose chemical composition is $(Mg_{0.9}Fe_{0.1})_2SiO_4$, adding 1% of liebenbergite would increase the density of $(Mg_{0.9}Fe_{0.1})_2SiO_4$ olivine by 0.4%.

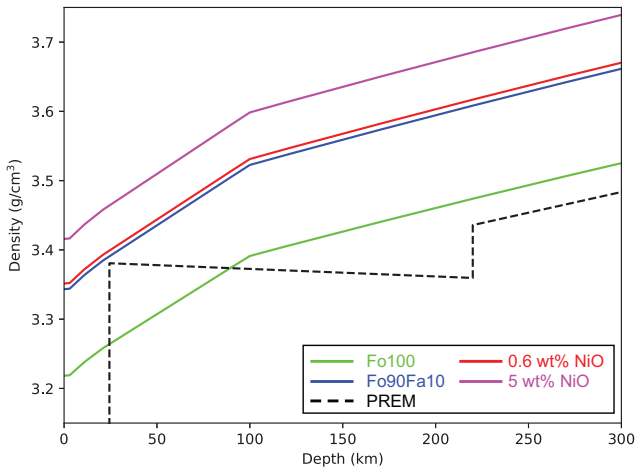

FIGURE 5. Calculated densities of olivines with different chemical compositions as functions of the depth in the upper mantle conditions. Green solid line = Mg_2SiO_4 (Fo_{100}). Blue solid line = $(Mg_{0.9}Fe_{0.1})_2SiO_4$ ($Fo_{90}Fa_{10}$, typical upper mantle olivine composition). Red solid line = $(Mg_{0.895}Fe_{0.099}Ni_{0.006})_2SiO_4$ (0.6 wt% NiO, upper bound of NiO concentration in olivine phenocrysts of the Hawaiian tholeiitic lava, Lynn et al. 2017). Magenta solid line = $(Mg_{0.855}Fe_{0.095}Ni_{0.05})_2SiO_4$ (5 wt% NiO, upper bound of NiO concentration found in the peridotite xenolith from the Kamchatka volcanic arc in Russia, Ishimaru and Arai 2008). Black dashed line = upper mantle density profile of the PREM model. (Color online.)

FUNDING

This work was performed at GeoSoilEnviroCARS (Sector 13), Partnership for Extreme Crystallography program (PX^2), Advanced Photon Source (APS), and Argonne National Laboratory. GeoSoilEnviroCARS is supported by the National Science Foundation-Earth Sciences (EAR-1634415) and Department of Energy-Geosciences (DE-FG02-94ER14466). PX^2 program and the COMPRES-GSECARS gas loading system are supported by COMPRES under NSF Cooperative Agreement EAR-1661511. Use of the Advanced Photon Source was supported by the U.S. Department of Energy, Office of Science, Office of Basic Energy Sciences, under Contract No. DE-C02-6CH11357. Development of ATREX IDL software is supported under National Science Foundation Grant EAR-1440005. Use of the COMPRES-GSECARS gas loading system was supported by COMPRES and GSECARS. Participation of P.D. and Y.H. in this project were supported by NSF Grant EAR-1722969.

ACKNOWLEDGMENTS

We acknowledge associate editor Oliver Tschauner and technical editor Ross Angel for handling the manuscript and giving helpful feedbacks, and the two anonymous reviewers for the constructive comments. D.Z. acknowledges X. Pu (University of Michigan) and Z. Jing (SUSTC) for helpful discussions. The experimental data (IUCr CIF format) in this manuscript can be found in the supporting information.

REFERENCES CITED

Akaogi, M., Akimoto, S.I., Horioka, K., Takahashi, K.I., and Horiuchi, H. (1982) The system $NiAl_2O_4$-Ni_2SiO_4 at high-pressures and temperatures—Spinelloids with spinel-related structures. Journal of Solid State Chemistry, 44, 257–267.

Akimoto, S.-I., Fujisawa, H., and Katsura, T. (1965) The olivine-spinel transition in Fe_2SiO_4 and Ni_2SiO_4. Journal of Geophysical Research, 70, 1969–1977.

Allegre, C., Manhes, G., and Lewin, E. (2001) Chemical composition of the Earth and the volatility control on planetary genetics. Earth and Planetary Science Letters, 185, 49–69.

Anderson, O.L. (1982) The Earth's core and the phase diagram of iron. Philosophical Transactions of the Royal Society of London, Series A, 306, 21–35.

Anderson, D.L., and Anderson, O.L. (1970) The bulk modulus-volume relationship for oxides. Journal of Geophysical Research, 75, 3494–3500.

Andrault, D., Bouhifd, M.A., Itie, J.P., and Richet, P. (1995) Compression and amorphization of $(Mg,Fe)_2SiO_4$ olivines: an X-ray-diffraction study up to 70 GPa. Physics and Chemistry of Minerals, 22, 99–107.

Andrault, D., Bolfan-Casanova, N., Lo Nigro, G., Bouhifd, M.A., Garbarino, G., and Mezouar, M. (2011) Solidus and liquidus profiles of chondritic mantle: Implication for melting of the Earth across its history. Earth and Planetary Science Letters, 304, 251–259.

Armentrout, M., and Kavner, A. (2011) High pressure, high temperature equation of state for Fe_2SiO_4 ringwoodite and implications for the Earth's transition zone. Geophysical Research Letters, 38.

Angel, R.J. (2000) Equations of state. Reviews in Mineralogy and Geochemistry, 41, 35–59.

Angel, R.J., Gonzalez-Platas, J., and Alvaro, M. (2014) EosFit7c and a Fortran module (library) for equation of state calculations. Zeitschrift für Kristallographie, 229, 405–419.

Angel, R.J., Alvaro, M., and Nestola, F. (2018) 40 years of mineral elasticity: a critical review and a new parameterisation of equations of state for mantle olivines and diamond inclusions. Physics and Chemistry of Minerals, 45, 95–113.

Back, M., Birch, W.D., Bojar, H.-P., Carter, J., Ciriotti, M.E., de Fourestier, J., Dolivo-Dobrovolsky, D., Downs, R.T., Grew, E.S., Fascio, L., and others. (2017) The New IMA List of Minerals. International Mineralogical Association.

Bass, J.D., Weidner, D.J., Hamaya, N., Ozima, M., and Akimoto, S. (1984) Elasticity of the olivine and spinel polymorphs of Ni_2SiO_4. Physics and Chemistry of Minerals, 10, 261–272.

Baur, W. (1974) The geometry of polyhedral distortions. Predictive relationships for the phosphate group. Acta Crystallographica, B30, 1195–1215.

Bickmore, B.R., Craven, O., Wander, M.C., Checketts, H., Whitmer, J., Shurtleff, C., Yeates, D., Ernstrom, K., Andros, C., and Thompson, H. (2017) Bond valence and bond energy. American Mineralogist, 102, 804–812.

Birle, J.D., Gibbs, G.V., Moore, P.B., and Smith, J.V. (1968) Crystal Structures of Natural Olivines. American Mineralogist, 53, 807–824.

Bostrom, D. (1987) Single-crystal X-ray diffraction studies of synthetic Ni-Mg olivine solid solutions. American Mineralogist, 72, 965–972.

Brown, I.D., Klages, P., and Skowron, A. (2003) Influence of pressure on the lengths of chemical bonds. Acta Crystallographica, B59(4), 439–448.

Burns, R.G. (1973) The partitioning of trace transition elements in crystal structures: a provocative review with applications to mantle geochemistry. Geochimica et Cosmochimica Acta, 37, 2395–2403.

Campbell, F.E., and Roeder, P. (1968) The stability of olivine and pyroxene in the Ni-Mg-Si-O system. American Mineralogist, 53, 257–268.

Clague, D.A. (1987) Hawaiian xenolith populations, magma supply rates, and

development of magma chambers. Bulletin of Volcanology 49, 577–587.
De Waal, S.A., and Calk, L.C. (1973) Nickel Minerals from Barberton, South Africa: VI. Liebenbergite, a Nickel Olivine. American Mineralogist, 58, 733–735.
Dera, P., Zhuravlev, K., Prakapenka, V., Rivers, M.L., Finkelstein, G.J., Grubor-Urosevic, O., Tschauner, O., Clark, S.M., and Downs, R.T. (2013) High pressure single-crystal micro X-ray diffraction analysis with GSE_ADA/RSV software. High Pressure Research, 33, 466–484.
Dolomanov, O.V., Bourhis, L.J., Gildea, R.J., Howard, J.A.K., and Puschmann, H. (2009) OLEX2: a complete structure solution, refinement and analysis program. Journal of Applied Crystallography, 42, 339–341.
Downs, R.T., Zha, C.-S., Duffy, T.S., and Finger, L.W. (1996) The equation of state of forsterite to 17.2 GPa and effects of pressure media. American Mineralogist, 81, 51–55.
Dziewonski, A.M., and Anderson, D.L. (1981) Preliminary Reference Earth Model. Physics of the Earth and Planetary Interiors, 25, 297–356.
Fei, Y., Ricolleau, A., Frank, M., Mibe, K., Shen, G., and Prakapenka, V. (2007) Toward an internally consistent pressure scale. Proceedings of the National Academy of Sciences, 104, 9182–9186.
Finger, L.W., Hazen, R.M., and Yagi, T. (1979) Crystal structures and electron densities of nickel and iron silicate spinels at elevated temperature or pressure. American Mineralogist, 64, 1002–1009.
Finkelstein, G.J., Dera, P.K., Jahn, S., Oganov, A.R., Holl, C.M., Meng, Y., and Duffy, T.S. (2014) Phase transitions and equation of state of forsterite to 90 GPa from single-crystal X-ray diffraction and molecular modeling. American Mineralogist, 99, 35–43.
Fischer, R.A., Nakajima, Y., Campbell, A.J., Frost, D.J., Harries, D., Langenhorst, F., Miyajima, N., Pollok, K., and Rubie, D.C. (2015) High pressure metal–silicate partitioning of Ni, Co, V, Cr, Si, and O. Geochimica et Cosmochimica Acta, 167, 177–194.
Frost, D.J. (2008) The Upper Mantle and Transition Zone. Elements, 4, 171–176.
Gentile, A.L., and Roy, R. (1960) Isomorphism and crystalline solubility in the garnet family. American Mineralogist, 45, 701–711.
Griffin, W.L., Cousens, D.R., Ryan, C.G., Sie, S.H., and Suter, G.F. (1989) Ni in Chrome Pyrope Garnets—a New Geothermometer. Contributions of Mineralogy and Petrology, 103, 199–202.
Hart, S.R., and Davis, K.E. (1978) Nickel Partitioning between olivine and silicate melt. Earth and Planetary Science Letters, 40, 203–219.
Hazen, R.M. (1976) Effects of temperature and pressure on the crystal structure of forsterite. American Mineralogist, 61, 1280–1293.
——— (1977) Effects of temperature and pressure on the crystal structure of ferromagnesian olivine. American Mineralogist, 62, 286–295.
——— (1993) Comparative compressibilities of silicate spinels: Anomalous behavior of $(Mg, Fe)_2SiO_4$. Science, 259, 206–206.
Hazen, R.M., and Finger, L.W. (1979) Bulk modulus-volume relationship for cation-anion polyhedra. Journal of Geophysical Research 84(B12), 6723–6728.
Hazen, R.M., Downs, R.T., Finger, L.W., and Ko, J. (1993) Crystal chemistry of ferromagnesian silicate spinels: Evidence for Mg-Si disorder. American Mineralogist, 78, 1320–1323.
Hazen, R.M., Downs, R.T., and Finger, L.W. (1996) High-pressure crystal chemistry of $LiScSiO_4$: An olivine with nearly isotropic compression. American Mineralogist, 81, 327–334.
Herzberg, C. (1992) Depth and degree of melting of komatiites. Journal of Geophysical Research, 97(B4), 4521–4540.
——— (2006) Petrology and thermal structure of the Hawaiian plume from Mauna Kea volcano. Nature, 444, 605–609.
Herzberg, C., Vidito, C., and Starkey, N.A. (2016) Nickel-cobalt contents of olivine record origins of mantle peridotite and related rocks. American Mineralogist, 101, 1952–1966.
Ishimaru, S., and Arai, S. (2008) Nickel enrichment in mantle olivine beneath a volcanic front. Contributions to Mineralogy and Petrology, 156, 119–131.
Jollands, M.C., Burnham, A.D., O'Neill, H.St.C., Hermann, J., and Qian, Q. (2016) Beryllium diffusion in olivine: A new tool to investigate timescales of magmatic processes. Earth and Planetary Science Letters, 450, 71–82.
Korenaga, J., and Kelemen, P.B. (2000) Major element heterogeneity in the mantle source of the North Atlantic igneous province. Earth and Planetary Science Letters, 184, 251–268.
Kroll, H., Kirfel, A., and Heinemann, R. (2014) Axial thermal expansion and related thermophysical parameters in the Mg,Fe olivine solid-solution series. European Journal of Mineralogy, 26, 607–621.
Kudoh, Y., and Takéuchi, Y. (1985) The crystal structure of forsterite Mg_2SiO_4 under high pressure up to 149 kb. Zeitschrift für Kristallographie-Crystalline Materials, 171, 291–302.
Lager, G.A., and Meagher, E.P. (1978) High-temperature structural study of six olivines. American Mineralogist, 63, 365–377.
Li, J., and Agee, C.B. (1996) Geochemistry of mantle-core differentiation at high pressure. Nature, 381, 686–689.
Lin, C.C. (2001) High-pressure Raman spectroscopic study of Co- and Ni-olivines. Physics and Chemistry of Minerals, 28, 249–257.
Liu, L.G. (1975) Disproportionation of Ni_2SiO_4 to stishovite plus bunsenite at high-pressures and temperatures. Earth and Planetary Science Letters, 24, 357–362.
Liu, L., Bassett, W.A., and Takahashi, T. (1974) Isothermal compression of a spinel phase of Co_2SiO_4 and magnesian ilmenite. Journal of Geophysical Research, 79, 1171–1174.
Lynn, K.J., Shea, T., and Garcia, M.O. (2017) Nickel variability in Hawaiian olivine: Evaluating the relative contributions from mantle and crustal processes. American Mineralogist, 102, 507–518.
Mao, H.K., Takahashi, T., Bassett, W.A., Weaver, J.S., and Akimoto, S.I. (1969) Effect of pressure and temperature on the molar volumes of wüstite and of three $(Fe, Mg)_2SiO_4$ spinel solid solutions. Journal of Geophysical Research, 74, 1061–1069.
Mao, H.-K., Takahashi, T., and Bassett, W.A. (1970) Isothermal compression of the spinel phase of Ni_2SiO_4 up to 300 kilobars at room temperature. Physics of the Earth and Planetary Interiors, 3, 51–53.
Matzen, A.K., Baker, M.B., Beckett, J.R., and Stolper, E.M. (2013) The temperature and pressure dependence of nickel partitioning between olivine and silicate melt. Journal of Petrology, 54, 2521–2545.
——— (2017) The effect of liquid composition on the partitioning of Ni between olivine and silicate melt. Contributions to Mineralogy and Petrology, 172, 3.
McDonough, W.F. (2014) Compositional model for the earth's core. In K.K. Turekian, Ed., Treatise on Geochemistry (2nd ed.), pp. 559–577. Elsevier.
McDonough, W.F., and Sun, S.S. (1995) The composition of the Earth. Chemical Geology, 120, 223–253.
Meng, Y., Fei, Y., Weidner, D.J., Gwanmesia, G.D., and Hu, J. (1994) Hydrostatic compression of γ-Mg_2SiO_4 to mantle pressures and 700 K: Thermal equation of state and related thermoelastic properties. Physics and Chemistry of Minerals, 21, 407–412.
Mizukami, S., Ohtani, A., Kawai, N., and Ito, E. (1975) High-pressure X-ray diffraction studies on β-and γ-Mg_2SiO_4. Physics of the Earth and Planetary Interiors, 10, 177–182.
Momma, K., and Izumi, F. (2008) VESTA: a three-dimensional visualization system for electronic and structural analysis. Journal of Applied Crystallography, 41, 653–658.
Mysen, B.O. (1979) Nickel partitioning between olivine and silicate melt—Henry's Law Revisited. American Mineralogist, 64, 1107–1114.
Nestola, F., Boffa Ballaran, T., Koch-Müller, M., Balic-Zunic, T., Taran, M., Olsen, L., Princivalle, F., Secco, L., and Lundegaard, L. (2010) New accurate compression data for γ-Fe_2SiO_4. Physics of the Earth and Planetary Interiors, 183, 421–425.
Nestola, F., Nimis, P., Ziberna, L., Longo, M., Marzoli, A., Harris, J.W., Manghnani, M.H., and Fedortchouk, Y. (2011a) First crystal-structure determination of olivine in diamond: Composition and implications for provenance in the Earth's mantle. Earth and Planetary Science Letters, 305, 249–255.
Nestola, F., Pasqual, D., Smyth, J., Novella, D., Secco, L., Manghnani, M., and Negro, A.D. (2011b) New accurate elastic parameters for the forsterite-fayalite solid solution. American Mineralogist, 96, 1742–1747.
Ozima, M. (1976) Growth of nickel olivine single crystals by the flux method. Journal of Crystal Growth, 33, 193–195.
Palme, H., and O'Neill, H.St.C. (2014) Cosmochemical estimates of mantle composition. In K.K. Turekian, Ed., Treatise on Geochemistry (2nd ed.), pp. 1–39. Elsevier.
Poe, B.T., Romano, C., Nestola, F., and Smyth, J.R. (2010) Electrical conductivity anisotropy of dry and hydrous olivine at 8 GPa. Physics of the Earth and Planetary Interiors, 181, 103–111.
Pu, X., Lange, R.A., and Moore, G. (2017) A comparison of olivine-melt thermometers based on D_{Mg} and D_{Ni}: The effects of melt composition, temperature, and pressure with applications to MORBs and hydrous arc basalts. American Mineralogist, 102, 750–765.
Putirka, K., Ryerson, F.J., Perfit, M., and Ridley, W.I. (2011) Mineralogy and composition of the oceanic mantle. Journal of Petrology, 52, 279–313.
Qin, F., Wu, X., Zhang, D., Qin, S., and Jacobsen, S.D. (2017) Thermal equation of state of natural Ti-bearing clinohumite. Journal of Geophysical Research: Solid Earth, 122(11), 8943–8951.
Ringwood, A.E. (1959) On the chemical evolution and densities of the planets. Geochimica et Cosmochimica Acta, 15, 257–283.
——— (1962) Prediction and confirmation of olivine-spinel transition in Ni_2SiO_4. Geochimica et Cosmochimica Acta, 26, 457–469.
Rivers, M., Prakapenka, V.B., Kubo, A., Pullins, C., Holl, C.M., and Jacobsen, S.D. (2008) The COMPRES/GSECARS gas-loading system for diamond anvil cells at the Advanced Photon Source. High Pressure Research, 28, 273–292.
Robinson, K., Gibbs, G.V., and Ribbe, P.H. (1971) Quadratic Elongation: A quantitative measure of distortion in coordination polyhedra. Science, 172, 567–570.
Sato, H. (1977a) Nickel content of basaltic magmas: identification of primary magmas and a measure of the degree of olivine fractionation. Lithos, 10, 113–120.
Sato, Y. (1977b) Equation of state of mantle minerals determined through high-pressure X-ray study. High Pressure Research: Applications in Geophysics, 307–312.
Shannon, R.D. (1976) Revised effective ionic-radii and systematic studies of interatomic distances in halides and chalcogenides. Acta Crystallographica,

A32, 751–767.
Sharp, Z.D., Hazen, R.M., and Finger, L.W. (1987) High-pressure crystal-chemistry of monticellite, $CaMgSiO_4$. American Mineralogist, 72, 748–755.
Sheldrick, G.M. (2008) A short history of SHELX. Acta Crystallographica, A64, 112–122.
Siebert, J., Badro, J., Antonangeli, D., and Ryerson, F.J. (2012) Metal–silicate partitioning of Ni and Co in a deep magma ocean. Earth and Planetary Science Letters, 321-322, 189–197.
Sobolev, A.V., Hofmann, A.W., Kuzmin, D.V., Yaxley, G.M., Arndt, N.T., Chung, S.L., Danyushevsky, L.V., Elliott, T., Frey, F.A., Garcia, M.O., and others. (2007) The amount of recycled crust in sources of mantle-derived melts. Science, 316, 412–417.
Speziale, S., Duffy, T.S., and Angel, R.J. (2004) Single-crystal elasticity of fayalite to 12 GPa. Journal of Geophysical Research-Solid Earth, 109, B12202.
Straub, S.M., LaGatta, A.B., Pozzo, A.L.M.D., and Langmuir, C.H. (2008) Evidence from high-Ni olivines for a hybridized peridotite/pyroxenite source for orogenic andesites from the central Mexican Volcanic Belt. Geochemistry, Geophysics, Geosystems, 9, Q03007.
Thompson, R.M., and Downs, R.T. (2001) Quantifying distortion from ideal closest-packing in a crystal structure with analysis and application. Acta Crystallographica, B57, 119–127.
Wilburn, D., and Bassett, W. (1976) Isothermal compression of spinel (Fe_2SiO_4) up to 75 kbar under hydrostatic conditions. High Temperatures-High Pressures, 8, 343–348.
Will, G., Hoffbauer, W., Hinze, E., and Lauterjung, J. (1986) The compressibility of forsterite up to 300 kbar measured with synchrotron radiation. Physica B+C, 139, 193–197.
Xu, J., Zhang, D., Fan, D., Downs, R.T., Hu, Y., and Dera, P.K. (2017) Isosymmetric pressure-induced bonding increase changes compression behavior of clinopyroxenes across jadeite-aegirine solid solution in subduction zones. Journal of Geophysical Research: Solid Earth, 122, B13502.
Zha, C.-S., Duffy, T.S., Downs, R.T., Mao, H.-K., and Hemley, R.J. (1998) Brillouin scattering and X-ray diffraction of San Carlos olivine: direct pressure determination to 32 GPa. Earth and Planetary Science Letters, 159, 25–33.
Zhang, L. (1998) Single crystal hydrostatic compression of $(Mg,Mn,Fe,Co)_2SiO_4$ olivines. Physics and Chemistry of Minerals, 25, 308–312.
Zhang, D.Z., Hu, Y., and Dera, P.K. (2016a) Compressional behavior of omphacite to 47 GPa. Physics and Chemistry of Minerals, 43, 707–715.
Zhang, J.S., Hu, Y., Shelton, H., Kung, J., and Dera, P. (2016b) Single-crystal X-ray diffraction study of Fe_2SiO_4 fayalite up to 31 GPa. Physics and Chemistry of Minerals, 44, 171–179.
Zhang, D.Z., Dera, P.K., Eng, P.J., Stubbs, J.E., Zhang, J.S., Prakapenka, V.B., and Rivers, M.L. (2017) High pressure single crystal diffraction at PX^2. Journal of Visual Experiments, e54660.

Manuscript received June 9, 2018
Manuscript accepted December 21, 2018
Manuscript handled by Oliver Tschauner

Endnote:

[1]Deposit item AM-19-46680, Supplemental Material and CIF. Deposit items are free to all readers and found on the MSA website, via the specific issue's Table of Contents (go to http://www.minsocam.org/MSA/AmMin/TOC/2019/Apr2019_data/Apr2019_data.html).